Computers and Structures 222 (2019) 25–35

Contents lists available at ScienceDirect

Computers and Structures

journal homepage: www.elsevier.com/locate/compstruc

# Quadrilateral overlapping elements and their use in the AMORE paradigm

Junbin Huang, Klaus-Jürgen Bathe *

*Department of Mechanical Engineering, Massachusetts Institute of Technology, Cambridge, MA 02139, USA*

ARTICLE INFO

*Article history:*
Received 3 April 2019
Accepted 22 May 2019
Available online 4 July 2019

*Keywords:*
Finite elements
Overlapping elements
Meshing
Mesh distortions
Convergence
AMORE

ABSTRACT

We give the formulation of new 4-node overlapping quadrilateral finite elements and demonstrate their performance in several numerical examples. The elements are insensitive to mesh distortions and lead overall to accurate numerical solutions. We show how the quadrilateral elements are utilized in the AMORE scheme of "automatic meshing with overlapping and regular elements". Since in this paradigm the finite elements interior to the domain of analysis are undistorted regular elements and the distortion-tolerant overlapping elements are used for discretizations near the boundaries, high solution accuracy is achieved. This accuracy is obtained with much less effort for meshing than in traditional finite element analysis and with a reasonable computational expense.



## 1. Introduction

While finite element methods are abundantly used in engineering and the sciences, their use is still much restricted due to the effort expended on meshing [1].

To avoid the generation of a mesh, meshless methods were proposed in which the global solution fields are constructed using scattered points [2]. The method of finite spheres is one such method [3]. However, the effort required for the numerical integration in meshless methods that do not involve the setting of parameters for solution stability causes the approach to be computationally expensive and prevents their wide use in engineering practice [2–4].

In order to significantly reduce the effort of meshing for finite element analysis without increasing the computational expense, we proposed the use of overlapping finite elements in a scheme of meshing [4–7], now referred to as the AMORE paradigm for "automatic meshing with overlapping and regular elements". Mostly easy to generate regular, traditional elements are used but also overlapping finite elements are employed. In this way the cost of obtaining an effective mesh is much reduced. The first overlapping elements used in AMORE were the disks (in three-dimensional analysis, spheres) of the method of finite spheres and effective coupling schemes between traditional finite elements and overlapping elements were proposed [4,5].

Recently, the concept of overlapping finite elements was improved and a new triangular overlapping element was presented [6,7], in which the overlapping finite element method can be regarded as a combination of the traditional finite element method and the method of finite spheres. The new element formulation is much more effective than the meshless methods because the numerical integration can be as simple as for traditional elements, and the bandwidth of the governing matrices is as in traditional finite element analysis.

An important feature of the overlapping finite elements is that the nodal degrees of freedom are polynomials or any other suitable functions, e.g. trigonometric functions can be included for the solution of wave propagation problems [8]. As a result, the overlapping finite elements can exactly represent the functions used as degrees of freedom irrespective of whether the mesh is distorted. This feature also pertains to the finite element method with interpolation covers [9], which however was only used in meshes of triangular elements, and the new overlapping elements are more effective [6,7].

Of course, meshes of overlapping finite elements satisfy the partition of unity property as do the formulations of the traditional, extended and generalized finite element methods [10–13], and there are similarities in these formulations. However, to have an effective finite element scheme, the details of the formulation are important. The AMORE scheme with the overlapping finite elements has been formulated to have stable, accurate and computationally efficient finite element solutions.

* Corresponding author.
*E-mail address:* kjb@mit.edu (K.J. Bathe).

https://doi.org/10.1016/j.compstruc.2019.05.011
0045-7949/

The AMORE paradigm for finite element analysis is deemed to be used directly on geometries obtained from computer-aided design programs or three-dimensional computerized scans. The main part of the domain (the interior) is discretized with regular traditional elements, and the boundary regions are meshed with overlapping elements. Since the overlapping elements are insensitive to mesh distortions, the complete mesh can be created quite effectively. An example is given in Section 3.4.

In this paper we present the formulation of novel quadrilateral overlapping finite elements for two-dimensional analyses, show their performance in several numerical examples, and illustrate their use in the AMORE paradigm.

## 2. The quadrilateral overlapping elements

The quadrilateral overlapping element is considered to be the overlapped region of four polygonal elements, as shown in Fig. 1. For each polygonal element, e.g. $D_I$, the interpolation is based on the method of finite spheres (disks in two-dimensional analyses) with the centers of the disks at the nodes. The final displacement field in the new 4-node element is the weighted average of the four method of finite spheres fields corresponding to the disks located at the four nodes of the element. The weight functions are the traditional shape functions. These concepts are used in the formulation of the 3-node elements [7,14] and are also the basis of the formulation of the new 4-node quadrilateral element.

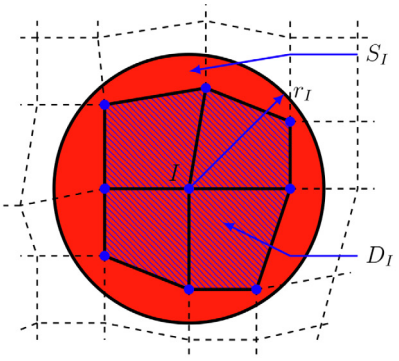


(a) A typical 9-node polygonal element $D_I$ and its local support $S_I$

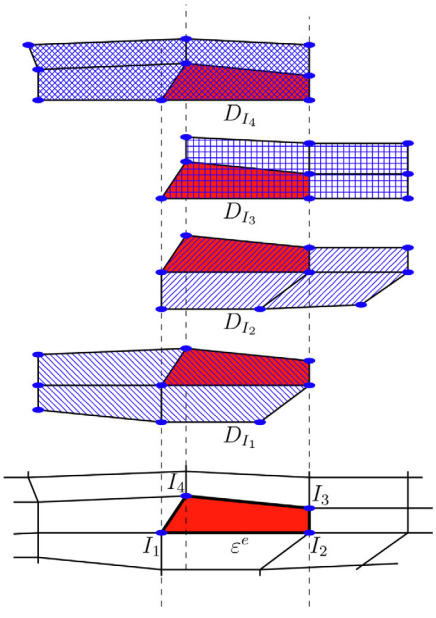


(b) A typical quadrilateral element obtained as the overlapped region $\varepsilon^e$

**Fig. 1.** The 4-node quadrilateral overlapping finite element.

### 2.1. The interpolation

We consider the solution of the displacement field of a well-posed problem in elasticity. The element interpolation of one component $u$ (say, the $x$-displacement) is given in the following form

$$u(\mathbf{x}) = \sum_{I=1}^{4} \rho_I(\mathbf{x})\, u_I(\mathbf{x}) \tag{1}$$

where the $\rho_I(\mathbf{x})$ are the new interpolation functions of the element. In traditional finite element analysis, $u_I$ is the nodal value of the field $u$ at node $I$. For the new overlapping finite elements, however, we use functions and usually polynomials as nodal unknowns, i.e. $u_I$ is a polynomial function given in the Cartesian coordinate system $\mathbf{x} = (x, y)$ attached to node $I$

$$u_I(\mathbf{x}) = a_{I1} + a_{I2}x + a_{I3}y + \cdots \tag{2}$$

If the linear basis is used, we have $u_I(\mathbf{x}) = a_{I1} + a_{I2}x + a_{I3}y$. Using the quadratic basis, $u_I(\mathbf{x}) = a_{I1} + a_{I2}x + a_{I3}y + a_{I4}x^2 + a_{I5}xy + a_{I6}y^2$. Since we use local Cartesian coordinates at node $I$, we have $a_{I1} = u_I(\mathbf{0})$. We will see that the $\rho_I$ are cubic functions in each of the isoparametric coordinates $(r, s)$ and we use the quadratic basis in the present paper; however the linear, cubic or even quartic polynomial bases might be used. In these cases, the computational effort required for a given accuracy would need to be assessed.

Comparing this interpolation with the approach of meshless interpolations we see that the nodal coupling leading to the bandwidth is as in traditional finite element analyses, while in meshless interpolations, the bandwidth of the stiffness matrix can be very large. Hence the discretization using Eq. (1) is computationally not expensive in solving the governing equations, see also Ref. [7].

To formulate the expression for the new interpolation functions in Eq. (1), we use (see Fig. 1)

$$u = \sum_{I=1}^{4} h_I \psi_I \tag{3}$$

where the $h_I$ are the traditional shape functions for a quadrilateral element, and the $\psi_I$ are functions that we establish using the concepts of the method of finite spheres. However, we can note already that since the traditional element interpolation functions $h_I$ provide a compatible displacement field, Eq. (3) does so too provided the functions $\psi_I$ are continuous in the corresponding polygonal element.

### 2.2. The functions $\psi_I$

We aim to construct for each node $I$ the function $\psi_I$ and consider for this purpose the polygonal element formed by all triangular and quadrilateral elements coupling into node $I$. A typical polygonal element is shown in Fig. 2, where we note that also two triangular subdomains are included. We define the support set $N_I$ for

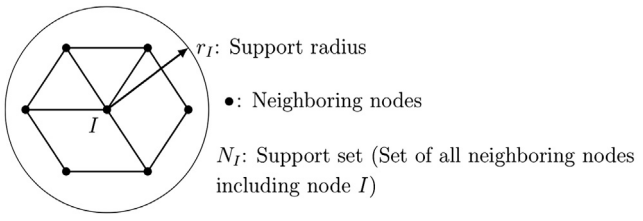


**Fig. 2.** Local support of the polygonal element.

node $I$ as the set of all nodes neighboring node $I$ and node $I$ itself. Fig. 2 also shows the support radius $r_I$, which is defined as the radius of a disk (a sphere in three-dimensional analysis) that contains all these nodes.

In this paper, the value of $r_I$ is given by

$$r_I = \max_{J \in N_I} \| \mathbf{x}_I - \mathbf{x}_J \| \tag{4}$$

and we also define another radius for each node by

$$r_I^* = \min_{J \in N_I,\ J \neq I} \| \mathbf{x}_I - \mathbf{x}_J \| \tag{5}$$

which will be used later on. With $r_I$ given we can define

$$\psi_I(\mathbf{x}) = \sum_{K=1}^{4} \phi_K^I(\mathbf{x}) u_K(\mathbf{x}) \tag{6}$$

where we use for $\phi_K^I$ the Shepard functions interpolated over the 4-node element of interest such as to provide compatibility.

The Shepard functions are widely used for interpolations of scattered data, and they are also adopted in the method of finite spheres. However, they are non-polynomial functions in the form of a quotient of polynomial weight functions. For this reason, when used in meshless techniques (like in the method of finite spheres), their use is computationally expensive, that is, a very high order numerical integration is needed [3,6]. Therefore we interpolate the functions using polynomials to obtain a much more effective solution scheme.

### 2.3. Interpolation of the Shepard functions

As in the formulation of triangular elements [7], we use here also for the interpolation of each Shepard function mid-edge nodes as shown in Fig. 3 to obtain a more accurate representation of the function

$$\tilde{\phi}_j^I(\mathbf{x}) = \sum_{i=1}^{8} \hat{h}_i(\mathbf{x}) \hat{\phi}_{ji}^I \tag{7}$$

where $\tilde{\phi}_j^I$ is the approximation of the Shepard function, the $\hat{\phi}_{ji}^I$ are coefficients to be determined, and the $\hat{h}_i(\mathbf{x})$ are the traditional shape functions of the 8-node quadrilateral element.

Three criteria govern the determination of these coefficients:

- The interpolated Shepard functions should lead to a compatible displacement field between elements, which is a basic requirement of finite element methods.
- The interpolated Shepard functions should be partition of unity functions, i.e. $\sum_J \tilde{\phi}_j^I = 1$.
- The element interpolation should depend only on the four weight functions (see below) located at the four corner nodes of the quadrilateral element.

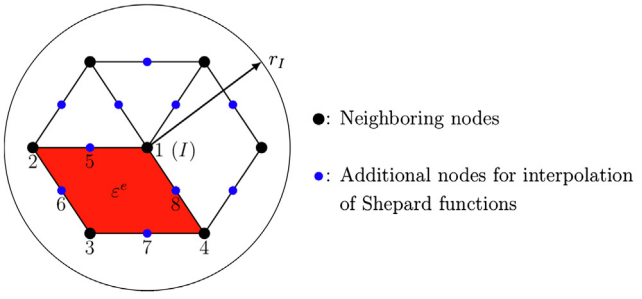


**Fig. 3.** Nodal positions (nodes 1, 2, 3, 4) of the Shepard functions and nodes used for the interpolation of the Shepard functions (nodes 1–8) for the quadrilateral 4-node element $\varepsilon^e$.

Based on these criteria we use the coefficients listed in Table 1, where the $W_J$ are the quartic spline weight functions:

$$W_J(\mathbf{x}) = \begin{cases} 1 - 6s^2 + 8s^3 - 3s^4, & 0 \leqslant s < 1 \\ 0, & s \geqslant 1 \end{cases} \tag{8}$$

with $s = d_J(\mathbf{x})/r_J$ being the scaled distance, and $d_J(\mathbf{x})$ being the distance between the point $\mathbf{x}$ and node $J$. The shapes of two typical weight functions are shown in Fig. 4.

To take mesh distortions into consideration, the final interpolated Shepard functions are given by

$$\phi_J^I = \frac{\sqrt{r_I^*}}{\sqrt{r_I} + \sqrt{r_I^*}} \tilde{\phi}_J^I + \frac{\sqrt{r_I}}{\sqrt{r_I} + \sqrt{r_I^*}} \delta_{IJ} \tag{9}$$

where the $r_I$ and $r_I^*$ are the radii defined in Eqs. (4) and (5), respectively, and $\delta_{IJ}$ is the Kronecker delta. For a severely distorted mesh, $r_I \gg r_I^*$, hence $\phi_J^I \approx \delta_{IJ}$, and the formulation reduces to using finite elements enriched by interpolation covers [9]. This method can exactly reproduce polynomial fields that are one order higher than the nodal basis functions used, hence a one order higher convergence can be achieved. However, quadrilateral finite elements enriched by interpolation covers may yield stiffness matrices that are only positive semi-definite, whereas the weight coefficients we use in Eq. (9) ensure a reasonable conditioning of the formulation.

With the above equations we now see that

$$\rho_I = \sum_{J=1}^{4} h_J \phi_I^J \tag{10}$$

**Table 1**
Interpolation of the Shepard functions on a quadrilateral element (see Fig. 3).

| | | | |
|---|---|---|---|
| $\hat{\phi}_1^I = \sum_{i=1}^{8} \hat{h}_i \hat{\phi}_{1i}^I$ | | | |
| $\hat{\phi}_{11}^I$ 1 | $\hat{\phi}_{12}^I$ $\frac{W_1}{W_1+W_2}\Big\|_{\mathbf{x}_2}$ | $\hat{\phi}_{13}^I$ 0 | $\hat{\phi}_{14}^I$ $\frac{W_1}{W_1+W_4}\Big\|_{\mathbf{x}_4}$ |
| $\hat{\phi}_{15}^I$ $\frac{W_1}{W_1+W_2}\Big\|_{\mathbf{x}_5}$ | $\hat{\phi}_{16}^I$ $\frac{W_1}{W_1+W_2+W_3}\Big\|_{\mathbf{x}_6}$ | $\hat{\phi}_{17}^I$ $\frac{W_1}{W_1+W_3+W_4}\Big\|_{\mathbf{x}_7}$ | $\hat{\phi}_{18}^I$ $\frac{W_1}{W_1+W_4}\Big\|_{\mathbf{x}_8}$ |
| $\hat{\phi}_2^I = \sum_{i=1}^{8} \hat{h}_i \hat{\phi}_{2i}^I$ | | | |
| $\hat{\phi}_{21}^I$ 0 | $\hat{\phi}_{22}^I$ $\frac{W_2}{W_1+W_2}\Big\|_{\mathbf{x}_2}$ | $\hat{\phi}_{23}^I$ 0 | $\hat{\phi}_{24}^I$ 0 |
| $\hat{\phi}_{25}^I$ $\frac{W_2}{W_1+W_2}\Big\|_{\mathbf{x}_5}$ | $\hat{\phi}_{26}^I$ $\frac{W_2}{W_1+W_2+W_3}\Big\|_{\mathbf{x}_6}$ | $\hat{\phi}_{27}^I$ 0 | $\hat{\phi}_{28}^I$ 0 |
| $\hat{\phi}_3^I = \sum_{i=1}^{8} \hat{h}_i \hat{\phi}_{3i}^I$ | | | |
| $\hat{\phi}_{31}^I$ 0 | $\hat{\phi}_{32}^I$ 0 | $\hat{\phi}_{33}^I$ 1 | $\hat{\phi}_{34}^I$ 0 |
| $\hat{\phi}_{35}^I$ 0 | $\hat{\phi}_{36}^I$ $\frac{W_3}{W_1+W_2+W_3}\Big\|_{\mathbf{x}_6}$ | $\hat{\phi}_{37}^I$ $\frac{W_3}{W_1+W_3+W_4}\Big\|_{\mathbf{x}_7}$ | $\hat{\phi}_{38}^I$ 0 |
| $\hat{\phi}_4^I = \sum_{i=1}^{8} \hat{h}_i \hat{\phi}_{4i}^I$ | | | |
| $\hat{\phi}_{41}^I$ 0 | $\hat{\phi}_{42}^I$ 0 | $\hat{\phi}_{43}^I$ 0 | $\hat{\phi}_{44}^I$ $\frac{W_4}{W_1+W_4}\Big\|_{\mathbf{x}_4}$ |
| $\hat{\phi}_{45}^I$ 0 | $\hat{\phi}_{46}^I$ 0 | $\hat{\phi}_{47}^I$ $\frac{W_4}{W_1+W_3+W_4}\Big\|_{\mathbf{x}_7}$ | $\hat{\phi}_{48}^I$ $\frac{W_4}{W_1+W_4}\Big\|_{\mathbf{x}_8}$ |

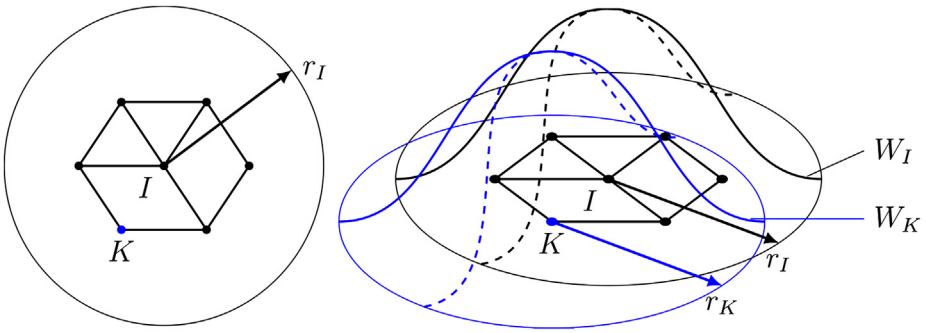


**Fig. 4.** Shapes of weight functions.

The new shape functions have contributions from both isoparametric and meshless interpolations. Hence the overlapping finite element method combines aspects of mesh-dependent and mesh-independent methods. We illustrate in the following sections that the new displacement interpolation results in accurate and distortion-insensitive numerical solutions.

### 2.4. Dirichlet boundary conditions

When using overlapping finite elements, the natural boundary conditions are imposed weakly as in traditional finite element methods [1]. To impose Dirichlet boundary conditions, a different set of interpolation is used for the boundary nodes that are constrained, namely we use the technique of interpolation covers [6,9].

Fig. 5 shows two typical cases of nodes on a boundary. As shown in Fig. 5(a), for a flat or curved boundary a local coordinate system is established at a boundary node $I_4$, with one axis tangent to and the other perpendicular to the displacement boundary. If the $u$ field is constrained along the $I_3 - I_4$ edge, we use, like in the method using interpolation covers, for the node $I = I_4$ the nodal displacement function

$$\psi_{I_4}(r,s) = u_{I_4} = a_{I_4 1} + a_{I_4 2} r + a_{I_4 3} rs + \text{ higher-order terms} \tag{11}$$

Thus, $\psi_{I_4}(0,s)$ becomes a constant as desired. Similarly, we can construct the function for node $I_3$. With the displacement field still given by Eq. (3), we see that if the Dirichlet boundary is flat, the constraints are imposed exactly, otherwise discretization errors occur.

For corner nodes, it can be seen in Fig. 5(b) that local axes are oriented along the corner edges, and similarly

$$\psi_{I_4}(r,s) = u_{I_4} = a_{I_4 1} + a_{I_4 2} rs + \text{ higher-order terms}$$

is used for a corner node $I_4$ with fixed boundary conditions.

### 2.5. The coupling between overlapping elements and traditional elements

In the AMORE paradigm, we use both overlapping elements and traditional elements to mesh the complete analysis domain; hence the coupling needs to be achieved, and for this purpose we formulate coupling elements.

We define that if all nodes of a quadrilateral element are overlapping element nodes, the element is an overlapping element, see Fig. 6. Similarly, if all nodes of a quadrilateral element are finite element nodes, the element is a traditional or regular finite element. Otherwise it is a coupling element.

The interpolation for a coupling element is still given by Eq. (3) but the $\psi_I$ are defined differently. For a coupling element, we denote the set of finite element nodes as $\Lambda_{\text{FE}}$, and the set of overlapping element nodes as $\Lambda_{\text{OFE}}$ with the union of these two sets equal to all nodes of the element. The interpolation $\psi_I$ for each node of the element is given by

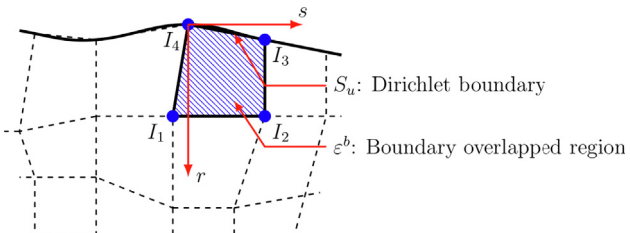


a) Curved or flat boundary

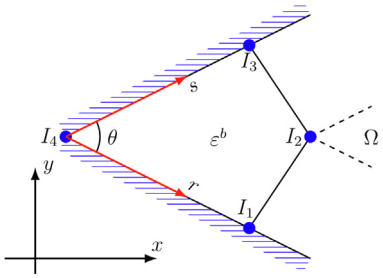


b) Corner node

**Fig. 5.** The local coordinate systems.

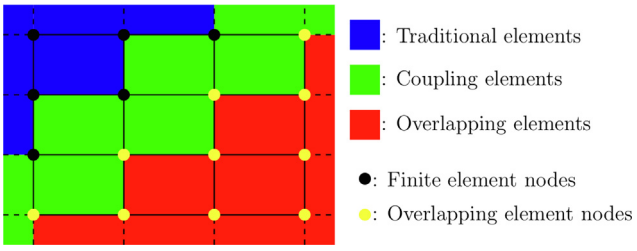


**Fig. 6.** Coupling of overlapping elements and finite elements.

$$\psi_I(\mathbf{x}) = \begin{cases} \alpha, & I \in \Lambda_{\text{FE}} \\ \sum_{K\in\Lambda_{\text{OFE}}} \phi_K^I u_K + \sum_{K\in\Lambda_{\text{FE}}} \phi_K^I \alpha, & I \in \Lambda_{\text{OFE}} \end{cases} \tag{12}$$

with

$$\alpha = \sum_{K\in\Lambda_{\text{OFE}}} h_K a_{K1} + \sum_{K\in\Lambda_{\text{FE}}} h_K u_K \tag{13}$$

where $a_{K1}$ is the constant part of the nodal unknown polynomial for node $K$. Since $\sum_{K\in\Lambda_{\mathrm{OFE}}} h_K a_{K1} + \sum_{K\in\Lambda_{\mathrm{FE}}} h_K u_K$ is independent of the index $I$, we denote it as $\alpha$. If $\Lambda_{\mathrm{FE}} = \varnothing$, the interpolation for a coupling element coincides with that of the "pure" overlapping element and if $\Lambda_{\mathrm{OFE}} = \varnothing$, we have the traditional finite element interpolation.

### 2.6. Mesh distortion sensitivity and convergence rates

The overlapping elements with or without coupling elements and tradtional finite elements satisfy the patch tests. Further, if the overlapping finite elements use the $k$th order basis, the elements are able to exactly represent any $k$th order polynomial irrespective of whether the mesh is distorted.

Namely, we can choose all nodal polynomials to be $p_k$ and have in each element

$$u(\mathbf{x}) = \left(\sum_{I=1}^{4} \rho_I\right) p_k \tag{14}$$

But

$$\sum_{I=1}^{4} \rho_I = \sum_{I=1}^{4} \sum_{J=1}^{4} h_I \phi_J^I = 1 \tag{15}$$

where we use the equality $\sum_{J=1}^{4} \phi_J^I = 1$ because the interpolated Shepard functions are designed to satisfy this criterion and will always do so, irrespective of any mesh distortion, hence

$$u(\mathbf{x}) = p_k$$

over the complete analysis domain. This conclusion is quite different from what we see with higher-order traditional finite elements, especially elements in the Serendipity family, that are (to a small or large degree) sensitive to mesh distortions [1].

To establish the rate of convergence we follow the usual arguments used in traditional finite element analysis [1]. We use the energy norm or equivalently the $H^1$ semi-norm ($|\cdot|_1$) for the error estimation. Considering a mesh of overlapping elements equipped with the $k$th order basis, the interpolation error satisfies

$$\inf_{u^*\in V^h} |u - u^*|_1 \leqslant c h^k \tag{16}$$

provided the exact solution $u$ has bounded derivatives up to the order $(k+1)$, where $V^h$ is the finite element discretized space, $u^*$ is an element in $V^h$, $h$ is the element size, and $c$ is a constant independent of $h$. Then, due to Céa's lemma, the numerical error satisfies

$$|u - u_h|_1 \leqslant c^* h^k \tag{17}$$

where $u_h$ is the numerical solution and $c^*$ is a constant independent of $h$.

To prove that Eq. (16) holds we use the usual interpolation theory [1]. Some numerical examples regarding the mesh distortion sensitivity and convergence rates are given in Section 3.

### 2.7. Numerical implementation

In the overlapping finite element method, the coefficients of the terms in the nodal polynomials are the unknowns. Since the coefficients corresponding to different polynomial terms are of different scales, the stiffness matrix may become ill-conditioned. To reduce the condition number of the resulting stiffness matrix, the nodal polynomials are rewritten as

$$u_I = a_{I1}^* + a_{I2}^* \frac{2x}{r_I} + a_{I3}^* \frac{2y}{r_I} + a_{I4}^* \frac{4x^2}{r_I^2} + a_{I5}^* \frac{4xy}{r_I^2} + a_{I6}^* \frac{4y^2}{r_I^2} + \cdots \tag{18}$$

and these new coefficients $a_{Ij}^*$ are solved for instead. This normalization results in a much better conditioning of the stiffness matrix.

In this paper, we use the 16-point quadrature rule (see Refs. [1,15,16]) for triangular overlapping elements and the $6 \times 6$ Gauss quadrature rule for quadrilateral overlapping elements. With these integration orders, the overlapping elements are evaluated exactly when they are not distorted [1]. The numerical effort for integration is actually a small part of the total expense [7,8]. We also note that $5 \times 5$ quadrature points for quadrilaterals and 12 quadrature points for triangles lead to no spurious mode, and in our example analyses the numerical solutions are almost the same.

## 3. Numerical examples

We give here some example solutions to illustrate the performance of the overlapping elements.

### 3.1. Thin beam problem to test trapezoidal elements

We consider the solution of the thin beam studied by MacNeal, see Fig. 7. MacNeal showed that any traditional 4-node finite element would either fail to pass the constant strain patch tests or suffer from trapezoidal locking [17]. The numerical solutions obtained with the quadrilateral overlapping element, the 4-node element with incompatible modes [18], and the traditional 4-node finite element are compared in Table 2. The results presented here are slightly better than those earlier reported, see Ref. [14], because to improve the formulation now Eq. (9) is used.

The incompatible element is designed for beam bending problems as bending solutions are added into the interpolation, but the overlapping elements are even more effective in this special problem, in particular when the mesh is distorted. In the solutions we refine the mesh by dividing each element edge into equal line segments. The reference solution is calculated using Timoshenko beam theory [19].

We see that the incompatible element suffers from trapezoidal locking but converges to the analytical solution as the mesh is refined. On the other hand, the 4-node isoparametric element does not perform well.

### 3.2. Convergence study for an "ad-hoc problem"

We consider the ad-hoc problem described in Fig. 8 [1]. The displacements are prescribed and the body force is calculated from the equations of equilibrium. The reference strain energy = $5.9414 \times 10^8$.

The numerical predictions of the strain energy are plotted in Fig. 9. The convergences obtained agree with our discussion in Section 2.6.

### 3.3. Study of effects of mesh distortions in bending beam problems

We give the solutions of two simple problems to illustrate the observations given in Section 2.6. As shown in Fig. 10, a beam is meshed with two elements. Pure bending and linear bending conditions are considered. The mesh distortion is parameterized by $e$. The analytical displacement solutions based on linear elasticity for these problems are [19]

$$\begin{aligned} &\text{Pure bending}: && u_x = \tfrac{120x-120xy}{E},\ u_y = \tfrac{60x^2+18y^2-36y}{E} \\ &\text{Linear bending}: && u_x = \tfrac{6x^2y-4.6y^3-6x^2-120xy+13.8y^2+120x-9.2y}{E} \\ & && u_y = \tfrac{-2x^3-1.8xy^2+60x^2+3.6xy+18y^2+9.2x-36y}{E} \end{aligned} \tag{19}$$

Using the traditonal 4-node finite element and the 4-node incompatible modes element, the mesh is further refined into $4 \times 4 \times 2$ elements by dividing each element edge into four equal

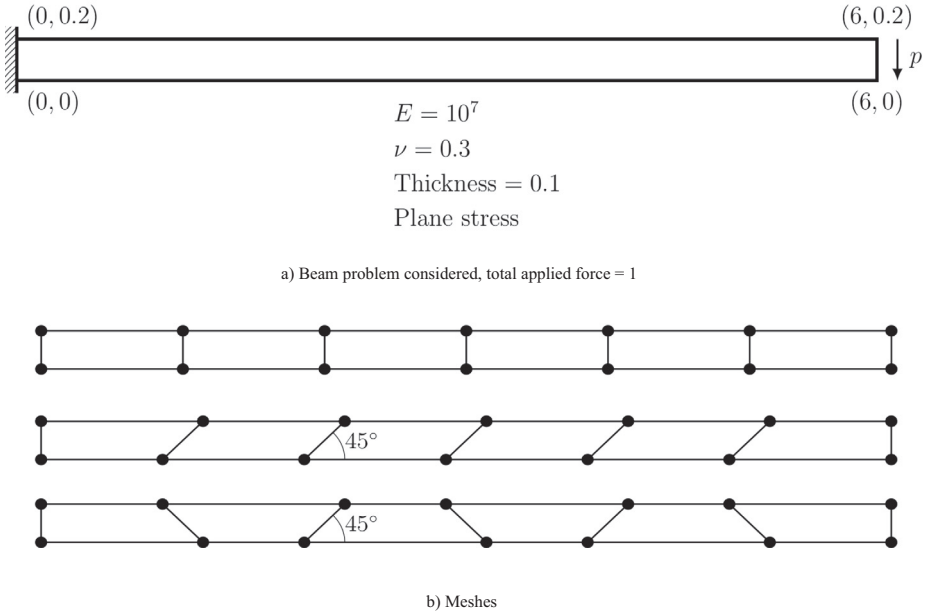


**Fig. 7.** Thin beam problem and meshes used.

**Table 2**
Numerical solutions of the thin beam problem (Reference solution = 0.1081).

| | 1 × 6 Mesh | 2 × 12 Mesh | 3 × 18 Mesh | 4 × 24 Mesh |
|---|---|---|---|---|
| *Overlapping finite element (Quadratic basis)* | | | | |
| Rectangular | 0.1069 (156 dofs) | – | – | – |
| Parallelogram | 0.1072 (156 dofs) | – | – | – |
| Trapezoidal | 0.1070 (156 dofs) | – | – | – |
| *Incompatible element* | | | | |
| Rectangular | 0.1073 (24 dofs) | – | 0.1076 (144 dofs) | 0.1077 (240 dofs) |
| Parallelogram | 0.0675 (24 dofs) | – | 0.1056 (144 dofs) | 0.1072 (240 dofs) |
| Trapezoidal | 0.0049 (24 dofs) | – | 0.0964 (144 dofs) | 0.1044 (240 dofs) |
| *4-node finite element* | | | | |
| Rectangular | 0.0101 (24 dofs) | – | – | 0.0671 (240 dofs) |
| Parallelogram | 0.0037 (24 dofs) | – | – | 0.0395 (240 dofs) |
| Trapezoidal | 0.0029 (24 dofs) | – | – | 0.0502 (240 dofs) |

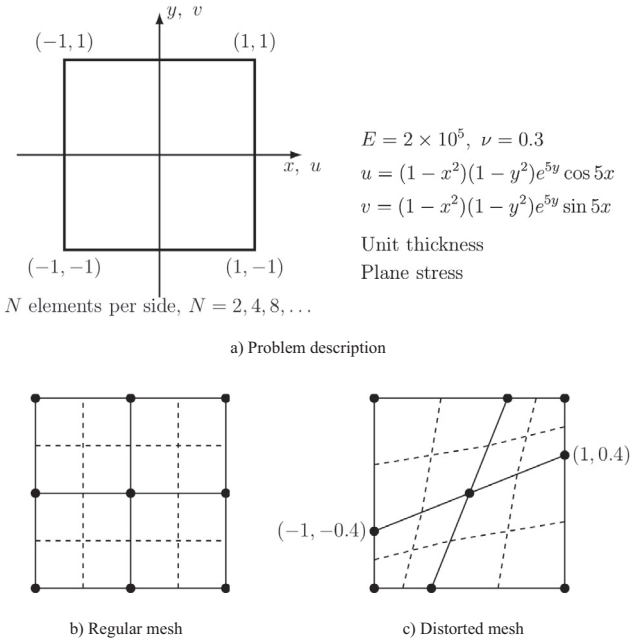


**Fig. 8.** The ad-hoc problem.

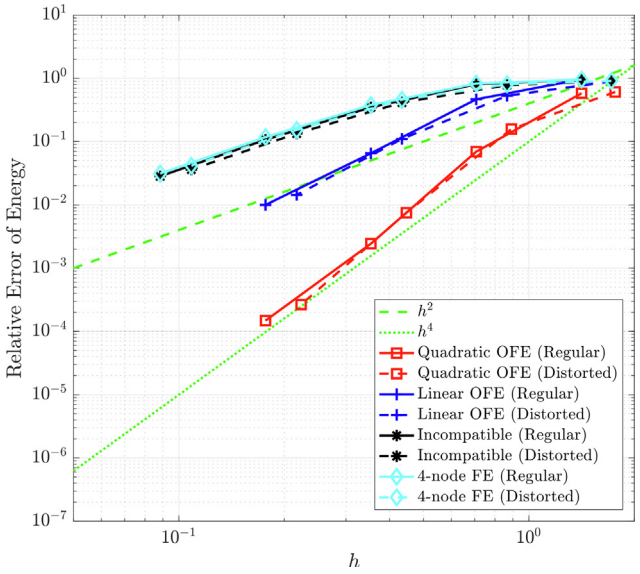


**Fig. 9.** The ad-hoc problem: convergence rates; $h$ is the mean element size (diameter of smallest circle encompassing the element) [1].

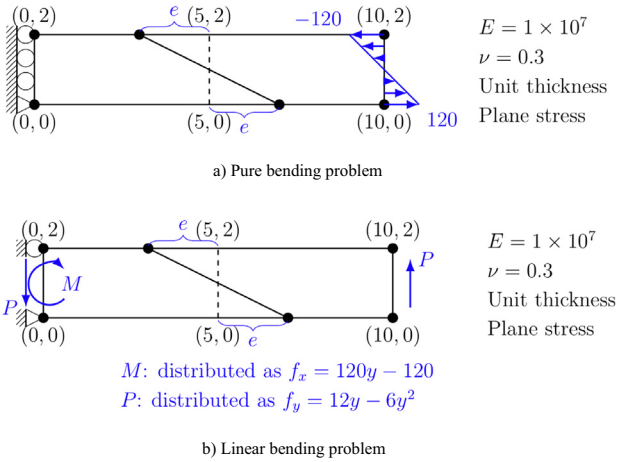


**Fig. 10.** A beam meshed with two elements.

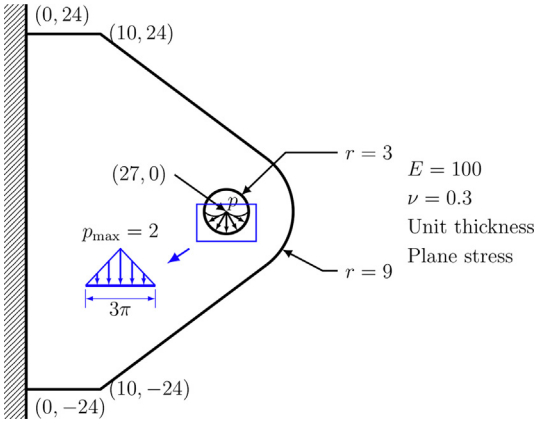


**Fig. 11.** The bracket problem.

segments. The numerical solutions of the vertical displacement at the point (10,0) are listed in Tables 3 and 4 as the distortion parameter increases.

In the pure bending case, the quadratic overlapping finite elements give the exact solution irrespective of the mesh distortion because the quadratic field of the analytical solution can always be reproduced. However the incompatible modes element shows sensitivity to the mesh distortion as the exact bending functions can only be represented when the element is undistorted. The 4-node finite element is most sensitive to the mesh distortion because it can only reproduce linear fields. In the linear bending case, although the cubic field cannot be exactly reproduced by the quadratic overlapping finite element, the numerical solutions are still very close to the analytical solution irrespective of the mesh distortion.

### 3.4. The AMORE paradigm in the analysis of a bracket problem

We show in this section how the quadrilateral overlapping element can be used in the AMORE paradigm. As shown in Fig. 11, a bracket is fixed on part of its boundary and loaded on the boundary of its hole.

In the AMORE scheme we use both regular and overlapping elements to simplify the meshing process. The overlapping elements are important because, being insensitive to mesh distortions, they are used in the areas difficult to mesh with regular elements. The AMORE paradigm involves these steps (see Fig. 12):

- The complete analysis domain is immersed in a Cartesian grid.
- The boundary is meshed. The cells located outside the domain or cutting the boundary are deleted.
- The remaining cells internal to the domain are converted into regular, that is, traditional finite elements. Instead of using 4-node finite elements as in previous examples using AMORE, we use here the incompatible modes element.
- The empty space in the domain is meshed using overlapping elements.

As seen in Fig. 12, we use both quadrilateral and triangular overlapping elements. The triangles are used for the boundary with large curvature. Because severely distorted elements are allowed, the mesh pattern follows very simple rules. The formulation of the triangular overlapping element used here is slightly different from the earlier formulation [7,14] to provide compatibility between the quadrilateral and triangular overlapping elements (see Appendix A).

We label in Fig. 12 elements with different colors. The regular elements are blue, the overlapping elements are red, and the coupling elements are green. The traditional mesh used for solution comparisons is also given. In this problem, we use quadratic overlapping elements. The reference solution is obtained using a fine traditional 9-node element mesh with over 340,000 degrees of freedom.

The reference strain energy is 1.044. The AMORE paradigm and traditional mesh all give reasonable energy predictions at 1.042. Fig. 13 plots the field solutions for the horizontal

**Table 3**
The vertical displacement $u_y$ at $(10, 0)$: The pure bending beam (OFE = overlapping finite elements, FE = finite elements).

| | $e = 0$ | $e = 2$ | $e = 4$ | $e = 4.9$ |
|---|---|---|---|---|
| Quadratic OFE (65 dofs) | $6.0000 \times 10^{-4}$ | $6.0000 \times 10^{-4}$ | $6.0000 \times 10^{-4}$ | $6.0000 \times 10^{-4}$ |
| Incompatible FE (84 dofs) | $6.0000 \times 10^{-4}$ | $5.9741 \times 10^{-4}$ | $5.4826 \times 10^{-4}$ | $4.8066 \times 10^{-4}$ |
| 4-node FE (84 dofs) | $5.1861 \times 10^{-4}$ | $3.3018 \times 10^{-4}$ | $1.6362 \times 10^{-4}$ | $1.2214 \times 10^{-4}$ |
| Reference | $6.0000 \times 10^{-4}$ | | | |

**Table 4**
The vertical displacement $u_y$ at $(10, 0)$: The linear bending beam.

| | $e = 0$ | $e = 2$ | $e = 4$ | $e = 4.9$ |
|---|---|---|---|---|
| Quadratic OFE (69 dofs) | $4.0874 \times 10^{-4}$ | $4.0886 \times 10^{-4}$ | $4.0899 \times 10^{-4}$ | $4.0931 \times 10^{-4}$ |
| Incompatible FE (87 dofs) | $4.0766 \times 10^{-4}$ | $4.0573 \times 10^{-4}$ | $3.7196 \times 10^{-4}$ | $3.2252 \times 10^{-4}$ |
| 4-node FE (87 dofs) | $3.5059 \times 10^{-4}$ | $2.4361 \times 10^{-4}$ | $1.3642 \times 10^{-4}$ | $1.0495 \times 10^{-4}$ |
| Reference | $4.0920 \times 10^{-4}$ | | | |

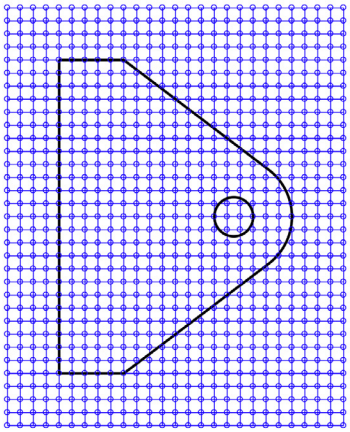

a) Step 1: The structure is immersed in a Cartesian grid

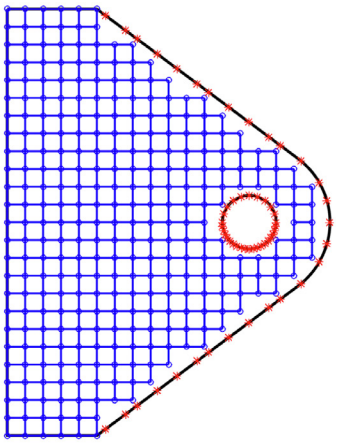

b) Step 2: The boundary is discretized; Cells outside or cutting the boundary are removed

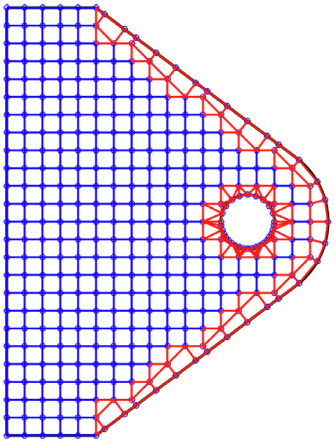

c) Step 3: The empty space is meshed

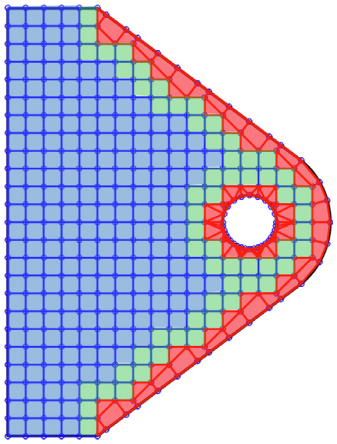

d) AMORE mesh (1936 dofs)

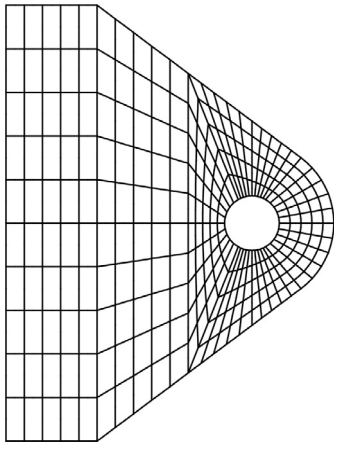

e) Traditional mesh (9-node elements; 2558 dofs)

**Fig. 12.** The AMORE paradigm in the solution of a bracket problem.

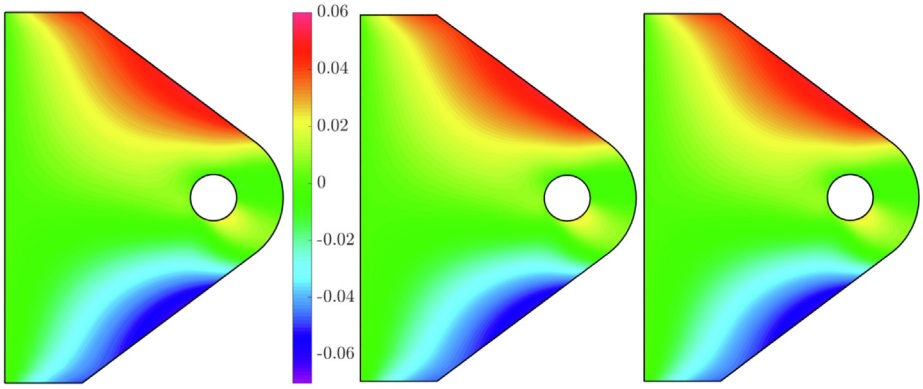


a) Left: AMORE mesh ($u_{max} = 0.05224, u_{min} = -0.06284$)
Middle: Traditional mesh ($u_{max} = 0.05224, u_{min} = -0.06298$)
Right: Reference solution ($u_{max} = 0.05231, u_{min} = -0.06312$)

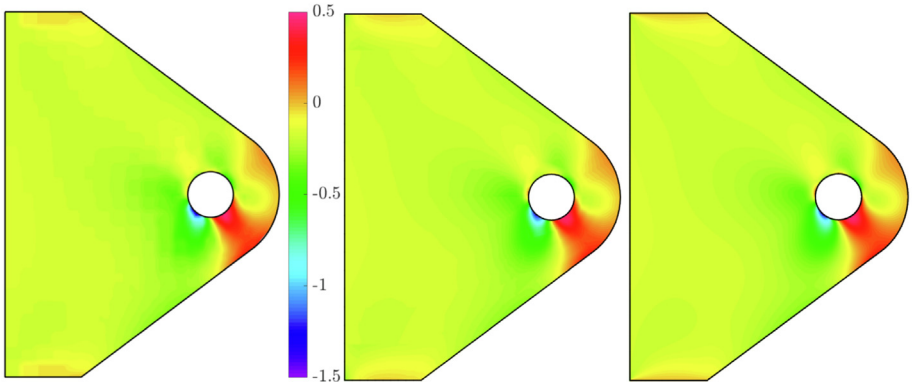


b) Left AMORE mesh ($\sigma_{xymax} = 0.4728, \sigma_{xymin} = -1.4525$)
Middle: Traditional mesh ($\sigma_{xymax} = 0.4625, \sigma_{xymin} = -1.3187$)
Right Reference solution($\sigma_{xymax} = 0.4680, \sigma_{xymin} = -1.4604$)

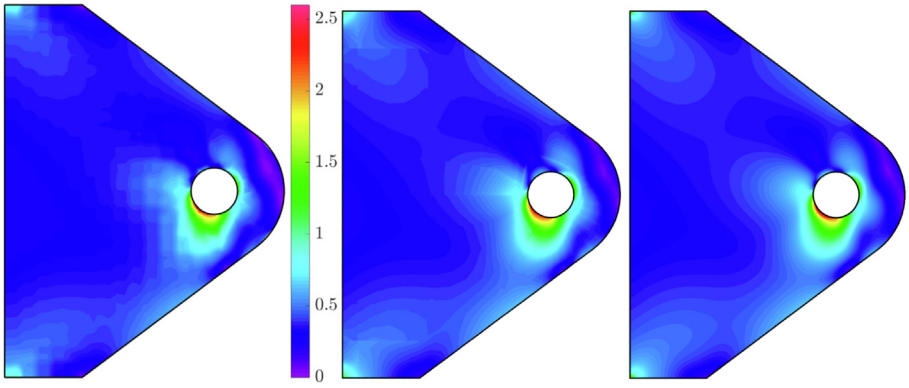


c) Left: AMORE mesh ($\bar{\sigma}_{max} = 2.6681$)
Middle: Traditional mesh ($\bar{\sigma}_{max} = 2.3358$)
Right: Reference solution ($\bar{\sigma}_{max} = 2.5800$)

**Fig. 13.** Numerical solutions for the bracket problem.

displacement $u$, the stress $\sigma_{xy}$, and the effective stress. The traditional mesh gives a good solution for the displacement field, however the stress predictions are not as good as when using the AMORE scheme.

## 4. Concluding remarks

We presented novel quadrilateral overlapping elements and illustrated their use. The overlapping elements are insensitive to

mesh distortions and in the problems tested give accurate solutions.

The displacement interpolation used in the formulation of the overlapping elements is based on the traditional isoparametric interpolation and the method of finite spheres. A major difference of the new elements from the traditional finite elements is that the nodal unknowns are polynomials (or other suitable functions) instead of single nodal values. According to the analysis needs, the order of the nodal polynomials can be increased and thus higher convergence rates can be achieved.

Since all polynomial terms in the nodal basis can be represented exactly even when the mesh is distorted, the new elements are insensitive to mesh distortions. Although the overlapping elements use the method of finite spheres interpolation, the Shepard functions are interpolated by polynomials. The numerical integration effort is reasonable and the nodal coupling for the resulting stiffness matrix is as in traditional finite element analysis which renders the proposed elements very effective.

Lower order quadrilateral overlapping finite elements still suffer from locking, which might be alleviated using the MITC interpolation [1]. The shear locking is well resolved in the above limited study given. However, a further study regarding a mixed formulation is needed and an optimal overlapping element formulation free of the locking effects should be pursued. The investigation should also include the inf-sup test [20].

The overlapping elements are developed to reduce the meshing effort for finite element analysis in the AMORE paradigm. We demonstrated the use of the AMORE scheme in one example. The new meshing paradigm is designed to be used for geometries established with any CAD program or by a computerized geometry scan. In the AMORE paradigm, typically most of the elements are regular, traditional elements, and overlapping elements are only used to establish the mesh near the boundaries. In the paper we focused on quadrilateral overlapping elements that correspond to the overlapped regions of polygons, like for the triangular overlapping elements [6,7]. However, a more general overlapping element scheme that allows elements to overlap "freely" in any geometric form as visualized in Refs. [4,14] would be very valuable.

The AMORE paradigm is promising because it enables fast automatic meshing, and the solution of the governing equations is effective. We see that the use of AMORE with overlapping elements opens an avenue for much valuable further research. More general and more effective overlapping elements may be sought [14], and the possibilities of using the paradigm in various analysis fields should be investigated.

## Appendix A

The triangular overlapping elements that we use with the quadrilateral elements are formulated in the way discussed for the quadrilateral overlapping elements. Each element is regarded as the overlapped region of three polygonal elements, and for each polygonal element $D_I$ we use the concepts of the method of finite spheres to establish the $\psi_I$ [6,14]. These fields are then assembled to obtain

$$u = \sum_{I=1}^{3} h_I \psi_I \tag{A.1}$$

where the $h_I$ are now the shape functions for the traditional 3-node triangular finite element.

We also have as in Eq. (6):

$$\psi_I(\mathbf{x}) = \sum_{K=1}^{3} \phi_K^I(\mathbf{x}) u_K(\mathbf{x}) \tag{A.2}$$

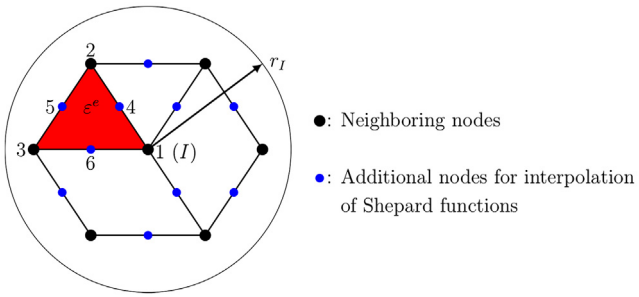


**Fig. A.1.** Interpolation of the Shepard functions on a triangular overlapped region $\varepsilon^e$.

**Table A.1**
Interpolation of the Shepard functions on a triangular element (see Fig. A.1).

| | | |
|---|---|---|
| $\hat{\phi}_1^I = \sum_{i=1}^{6} \hat{h}_i \hat{\phi}_{1i}^I$ | | |
| $\hat{\phi}_{11}^I$ 1 | $\hat{\phi}_{12}^I$ $\frac{W_1}{W_1+W_2}\Big\|_{\mathbf{x}_2}$ | $\hat{\phi}_{13}^I$ $\frac{W_1}{W_1+W_3}\Big\|_{\mathbf{x}_3}$ |
| $\hat{\phi}_{14}^I$ $\frac{W_1}{W_1+W_2}\Big\|_{\mathbf{x}_4}$ | $\hat{\phi}_{15}^I$ $\frac{W_1}{W_1+W_2+W_3}\Big\|_{\mathbf{x}_5}$ | $\hat{\phi}_{16}^I$ $\frac{W_1}{W_1+W_3}\Big\|_{\mathbf{x}_6}$ |
| $\hat{\phi}_2^I = \sum_{i=1}^{6} \hat{h}_i \hat{\phi}_{2i}^I$ | | |
| $\hat{\phi}_{21}^I$ 0 | $\hat{\phi}_{22}^I$ $\frac{W_2}{W_1+W_2}\Big\|_{\mathbf{x}_2}$ | $\hat{\phi}_{23}^I$ 0 |
| $\hat{\phi}_{24}^I$ $\frac{W_2}{W_1+W_2}\Big\|_{\mathbf{x}_4}$ | $\hat{\phi}_{25}^I$ $\frac{W_2}{W_1+W_2+W_3}\Big\|_{\mathbf{x}_5}$ | $\hat{\phi}_{26}^I$ 0 |
| $\hat{\phi}_3^I = \sum_{i=1}^{6} \hat{h}_i \hat{\phi}_{3i}^I$ | | |
| $\hat{\phi}_{31}^I$ 0 | $\hat{\phi}_{32}^I$ 0 | $\hat{\phi}_{33}^I$ $\frac{W_3}{W_1+W_3}\Big\|_{\mathbf{x}_3}$ |
| $\hat{\phi}_{34}^I$ 0 | $\hat{\phi}_{35}^I$ $\frac{W_3}{W_1+W_2+W_3}\Big\|_{\mathbf{x}_5}$ | $\hat{\phi}_{36}^I$ $\frac{W_3}{W_1+W_3}\Big\|_{\mathbf{x}_6}$ |

where the $\phi_K^I$ are the interpolated Shepard functions over the triangular element. As can be seen in Fig. A.1, we use 6 nodes to interpolate the Shepard functions.

We first interpolate the Shepard functions by

$$\tilde{\phi}_J^I(\mathbf{x}) = \sum_{i=1}^{6} \hat{h}_i(\mathbf{x}) \hat{\phi}_{Ji}^I \tag{A.3}$$

where naturally the $\hat{h}_i$ represent the shape functions for the 6-node traditional triangular finite element. The coefficients are listed in Table A.1.

Finally, the interpolated Shepard functions are given by

$$\phi_J^I = \frac{\sqrt{r_I^*}}{\sqrt{r_I} + \sqrt{r_I^*}} \tilde{\phi}_J^I + \frac{\sqrt{r_I}}{\sqrt{r_I} + \sqrt{r_I^*}} \delta_{IJ} \tag{A.4}$$

as in Eq. (9).

## References

[1] Bathe KJ. Finite element procedures. Prentice Hall; 1996. 2nd ed. KJ Bathe, Watertown, MA; 2014 and Higher Education Press, China; 2016.
[2] Liu GR. Meshfree methods: Moving beyond the finite element method. Taylor & Francis; 2009.
[3] De S, Bathe KJ. The method of finite spheres. Comput Mech 2000;25 (4):329–45.

[4] Bathe KJ. The finite element method with "overlapping finite elements". In: Zingoni A, editor. Proceedings sixth international conference on structural engineering, mechanics and computation – SEMC 2016. South Africa: Cape Town; 2016.
[5] Bathe KJ, Zhang L. The finite element method with overlapping elements – A new paradigm for CAD driven simulations. Comput Struct 2017;182:526–39.
[6] Zhang L, Bathe KJ. Overlapping finite elements for a new paradigm of solution. Comput Struct 2017;187:64–76.
[7] Zhang L, Kim KT, Bathe KJ. The new paradigm of finite element solutions with overlapping elements in CAD – Computational efficiency of the procedure. Comput Struct 2018;199:1–17.
[8] Kim KT, Zhang L, Bathe KJ. Transient implicit wave propagation dynamics with overlapping finite elements. Comput Struct 2018;199:18–33.
[9] Kim J, Bathe KJ. The finite element method enriched by interpolation covers. Comput Struct 2013;116:35–49.
[10] Melenk JM, Babuška I. The partition of unity finite element method: Basic theory and applications. Comput Methods Appl Mech Eng 1996;139(1–4):289–314.
[11] Strouboulis T, Copps K, Babuška I. The generalized element method. Comput Methods Appl Mech Eng 2001;190(32–33):4081–193.
[12] Bathe KJ, Almeida CA. A simple and effective pipe elbow element – Linear analysis. J Appl Mech, Trans ASME 1980;47(1):93–100.
[13] Belytschko T, Gracie R, Ventura G. A review of extended/generalized finite element methods for material modeling. Model Simul Mater Sci Eng 2009;17(4):043001.
[14] Bathe KJ. The AMORE paradigm for finite element analysis. Adv Eng Softw 2019;130:1–13.
[15] Cowper GR. Gaussian quadrature formulas for triangles. Int J Numer Methods Eng 1973;7(3):405–8.
[16] Dunavant DA. High degree efficient symmetrical Gaussian quadrature rules for the triangle. Int J Num Methods Eng 1985;21(6):1129–48.
[17] MacNeal RH. A theorem regarding the locking of tapered four-node membrane elements. Int J Numer Methods Eng 1987;24(9):1793–9.
[18] Ibrahimbegovic A, Wilson EL. A modified method of incompatible modes. Commun Appl Numer Methods 1991;7(3):187–94.
[19] Bucalem ML, Bathe KJ. The mechanics of solids and structures – Hierarchical modeling and the finite element solution. Springer; 2011.
[20] Bathe KJ. The inf-sup condition and its evaluation for mixed finite element methods. Comput Struct 2001;79(2):243–52.